Journal of Science and Technology – Engineering and Technology for Sustainable Development
Volume 35, Issue 4, October 2025, 024-032

The Influence of Oxidizer Content and Energy Additive on Thermal Decomposition and Burning Rate of High Energy-Carrying Composite Materials

Doan Anh Tuan[1,*], Nguyen Thanh Hung[2], Mai Thi Thu[3], Nguyen Tien Hoa[3], Hoang Minh Tuan[3], Dinh Van Hoan[3]
[1]*Institute of Theoretical and Applied Research, Duy Tan University, Ha Noi, Vietnam*
[2]*Hanoi University of Science and Technology, Ha Noi, Vietnam*
[3]*Viettel Aerospace Institute, Ha Noi, Vietnam*
[*]*Corresponding author email: tuan.lochoadaub.k54@gmail.com*

Abstract

During the course of this inquiry, an attempt has been made to understand the thermal decomposition characteristics and burning rate of ammonium perchlorate working as an oxidizer and polyvinyl chloride functioning as a fuel binder for high energy-carrying composite materials. The samples were examined for material morphology and elemental composition by scanning electron microscope and dispersive energy X-ray spectrometer methods. In addition, a NETZSCH simultaneous thermal analyzer comprising a differential scanning calorimeter and a thermogravimetric analyzer has also been utilized to ascertain the thermal decomposition method associated with each composition. The thermal decomposition process of the energy-carrying composite materials consisted of three distinct stages, and the mass loss rate during this process ranged from 100 °C to 500 °C, accounting for 99% of the sample mass. The enhanced catalytic activity of Fe_2O_3 in ECCMs significantly lowers the exothermic decomposition temperature and increases the total heat release. Besides, the burning rate studies have been conducted at ambient and different pressures with and without Fe_2O_3, providing valuable insights into the combustion behavior of ECCMs under varying conditions.

Keywords: High energy-carrying composite, thermal decomposition, burning rate, AP content, Fe_2O_3.

1. Introduction

In the new century, sophisticated composite material technology will experience accelerated development, providing substantial support for the advancement of new high-performance solid engines, thereby enabling a significant enhancement in engine performance. Energy-carrying composite materials (ECCMs) have significant benefits over other energy-carrying materials. Consequently, the research and development of ECCMs for propulsion in flying vehicles is an unavoidable trend in the fields of military science and space exploration thrust owing to their high energy density, compactness, operational readiness, reliability, cost-effectiveness, and storability. ECCMs are heterogeneous energetic materials composed of a polymeric matrix that a solid-phase amalgamation of oxidizer and fuel that generates the necessary energy for propulsion upon combustion. The polymeric matrix serves both as a structural component and as a source of fuel [1]. The oxidizer typically consists of ammonium perchlorate (AP) or other crystalline chemicals, comprising 60% to 80% of the total mass. The binder, which makes up around 10% to 15% of the total mass, is essential for maintaining the cohesion of the material components and preserving the integrity of the grain during combustion. Hydroxyl-terminated polybutadiene (HTPB) and polyvinyl chloride (PVC) are commonly employed as binders in ECCMs [2, 3]. The binder is crucial for preserving the structural stability of ECCMs, guaranteeing optimal combustion throughout operation. Aluminium or other metals can be incorporated into the ECCM mixture as a high-energy density fuel, with a mass percentage ranging from 0% to 20% of the total. The combustion process can be precisely adjusted by incorporating a tiny percentage of modifiers (such as burning catalysts, retarding agents, or coolants) and/or additives, which can enhance the blending (plasticizers, wetting agents, and curing catalysts) [4].

The composition and quantities of chemical constituents yield varying physical, chemical, mechanical, thermal, storage stability, danger, and combustion qualities. The selection criteria for ECCMs create a difficulty for designers, impacting mission performance. Significant work has been focused on comprehending the decomposition of AP and its rate of combustion. AP is a white crystalline compound having the chemical formula NH_4ClO_4. It is a potent oxidizing agent that remains stable at ambient temperature in its

p-ISSN 3093-3242
e-ISSN 3093-3579
https://doi.org/10.51316/jst.185.etsd.2025.35.4.4
Received: Nov 20; Revised: Mar 24, 2025;
Accepted: Apr 1, 2025; Online: Sep 20, 2025.

pure state, although decomposes at temperatures of 150 °C or above [5]. AP is a crucial element in ECCMs due to its oxidizing characteristics. When amalgamated with appropriate fuels, it generates a ECCM possessing a high energy density. However, there has been a lack of emphasis on investigating the decomposition of fuel binders. Furthermore, it is important to note that the fuel binder is accountable for retaining the particle oxidizer or metals within its structure. Any appropriate additive that can enhance the heat of combustion or pyrolysis rate of the fuel binder will consequently impact the entire burning rate of the ECCM [6]. Based on current knowledge of modern ECCM, it is necessary to have further information about the fuel binder disintegration mechanism and how it interacts with the oxidizer throughout the fuel combustion process. The significance of these reactions is contingent upon the makeup of the ECCMs and the prevailing environmental conditions. On the other hand, the combustion behavior of ECCM is frequently altered by including modifiers into its composition in modest amounts (less than 3 wt.%). Iron oxide and copper chromite are often used combustion modifiers in ECCMs to improve burning characteristics [4]. Hence, the thermal decomposition, combustion characteristics, and burning rate of the ECCMs can be modified by physical means, such as employing various AP compositions or incorporating additives with different burning catalysts.

The objective of this study is to examine the influence of the AP content and energy additive on the combustion of these ECCMs. This work aims to experimentally study the thermal decomposition, combustion behavior of AP/PVC-based ECCMs with different AP loading. Three distinct levels of AP oxidizer loading, specifically 60%, 70%, and 80% by weight, were utilized in each material composition. PVC was used as the fuel binder and AP served as the oxidizer. The PVC powder was supplemented with an equivalent quantity of dry dioctyl phthalate (DOP) in order to achieve the formation of a thick polymer substance. Additionally, aluminium was employed as an addition to enhance the energy density and particular impulse, while maintaining a constant content of 7 wt.%. This study also examined the impact of ferric oxide (Fe_2O_3) at a concentration of 1.5% by weight. Burning rate data have been generated for different pressures of 0.109 MPa, 2.595 MPa, 5.073 MPa, 6.395 MPa, and 7.993 MPa with and without Fe_2O_3. An attempt has also been made to examine the outcomes in respect to established theories and actual correlations of AP/PVC with and without Fe_2O_3, and to compare the findings. Our research highlights the effect of varying AP content on the combustion efficiency of ECCMs, the impact of catalytic activity of Fe_2O_3 in ECCMs as well as combustion behavior of ECCMs under varying conditions.

2. Experiment

2.1. Materials

AP procured from Calimara, India has been used as an oxidizer with a purity more than 99.5%. A bimodal particle distribution has been chosen to increase the oxidizer loading i.e. to increase the volumetric efficiency. The oxidizer particle size of about 45 µm to 200 µm has been used. The PVC resin and in commercial grade was obtained from LG Chem, Korea, in the form of white powder and was used after drying in oven been used. The purity plasticizer DOP was supplied by Merck, Germany. The aluminium powders used in this study are pure (more than 99.8%), spherical powders with mean diameters varying between 5 µm and 20 µm, supplied by Xian Function Material Group Co., Ltd. Ferric red oxide 101 ($Fe_2O_3.\alpha H_2O$) procured from Alfa Chemistry, China. The particle size of nano Fe_2O_3 used is 0.1 µm to incorporate in the polymer matrix, revealing a well-separated characteristic necklace-like structure of α-Fe_2O_3 particles at high magnification [7]. The ratio composition of the ECCMs has been given in Table 1.

Table 1. Formulation of ECCM samples (wt.%)

Sample	AP	PVC	DOP	Al	Fe_2O_3*
S1	60	16.5	16.5	7	-
S2	70	11.5	11.5	7	-
S3	80	6.5	6.5	7	-
S4	70	11.5	11.5	7	1.5

** by weight in all compositions of the sample*

The components used for the aforementioned compositions were stored in conditions of controlled humidity. All the mixing processes were conducted with consistent processing factors, including mixing duration, level of vacuum applied, mixer temperature, and order of component addition into the mixer. Prior to utilization, the oxidizer underwent a drying process at a temperature of 60 °C for a duration of one hour in order to eliminate any moisture present. The PVC and DOP were combined in a stainless-steel container, and then the necessary amounts of AP were added. A separate addition of a burning catalyst concentration of 1.5 wt.% of the total sample weight was made in the catalyzed compositions. The blending process was conducted for a duration of one hour at 150 °C in order to obtain the ultimate mixture by roll mill machine. The as-made plastic containers were placed in a vacuum electric oven at a temperature of 60 °C for a duration of five days to allow the ECCM to cure. Subsequently, the molds were extracted from the oven and left to cool down to the ambient temperature. They were then placed in a desiccator to prevent any moisture from being absorbed.

2.2. Characterization

Once the ECCMs were created, the surfaces were examined for differences that could be attributed to compositions of the samples. The physical detail of ECCM was detected by the scanning electron microscope (SEM) on a JEOL JCM-7000 Benchtop (Japan) with effective use of Low-Vacuum mode. To prevent beam damage to the sample and charging that affects the image, a modest accelerating voltage and current were employed. The chemical characteristics of the ECCM surface were also determined by the JEOL JCM-7000 Benchtop model SEM integrated with an Energy Dispersive X-ray Spectroscopy (EDS), which requires that the samples remain coated by Au to ensure conductive and accurate scans. The color mapping of elements unique to each part of the ECCM provides much-needed detail on the surface of the ECCM cross-section, which was also performed by EDS mapping.

Differential Scanning Calorimeter (DSC) measurements were performed using NETZSCH STA 449F5 (Germany). In the DSC measurements, samples weighing 5 mg were heated at a rate of 10 °C/min in specific pans from 100 °C to 500 °C under a static atmosphere of nitrogen at 20 mL/min. Thermogravimetric (TG) measurements were also carried out using a NETZSH thermal analyzer (model STA 449F5). Samples weighing about 10 mg were heated at a rate of 10 °C/min in the temperature range of 100 °C to 500 °C under a static atmosphere of nitrogen with a flow rate of 20 mL/min [8]. The sample was placed in a platinum crucible and then the lid has been closed for measurement. Simultaneous TG measures both heat flow (DSC) and weight changes (TG) in a material as a function of temperature or time in a controlled atmosphere. NETZCH program captured heat flow as a temperature function. Thermal decomposition data from several samples was interpreted using thermograms. Concurrent TG investigations calculate mass loss with temperature increase.

2.3. Burning Rate Studies

The Crawford test is also conducted to evaluate the burning rate of the ECCMs in analytical models of the combustion process and the burning rate. The conventional strand burner was employed to ascertain the combustion rates of AP as oxidizer and PVC as fuel binder-based ECCMs with and without Fe_2O_3 at 0.109 MPa, 2.595 MPa, 5.073 MPa, 6.395 MPa, and 7.993 MPa [2]. The chamber has been pressurized with nitrogen gas. The digital pressure sensors have been employed to document the pressures in chambers and lines and the incoming pressure. The arrangement includes a surge reservoir to guarantee that the chamber maintains a consistent pressure. This is evident in Fig. 1.

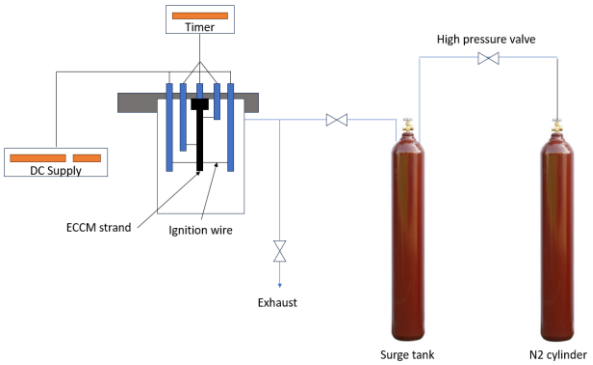

Fig. 1. Line diagram of ECCM strand

The ECCM strands were mounted in the chamber, with two finely drilled apertures at a distance of 5 cm to accommodate the fuse wires. The igniter wire was appropriately positioned at the apex of the strand. The lid was secured to the chamber with the inclusion of electrical connections. The chamber was subsequently pressurized to the necessary pressure using nitrogen gas. The strand was ignited to record time with the assistance of an electrical timer, and the requisite electrical connections were established. For each strand, a comparable methodology has been implemented. The time between the two fuse wires or break wires was then used to determine the combustion rates.

The Saint-Robert's Law or Vieille's Law is a formula to determine the rate of combustion of ECCMs. The general formula is:

$$r = aP^n \quad (1)$$

where r is the linear burning rate (mm/s); a is the coefficient related to the ECCM properties; P is the pressure (MPa); n is the pressure exponent. Collecting the coefficients a and n for Saint-Robert's Law (or Vieille's Law) involves experimental testing and regression analysis from experimental data for the burning rate r at different pressures P. Collecting a and n typically perform experiments to measure the burning rate at different pressures. By plotting the burning rate r against the pressure p on a log-log scale, then determine the values of a and n from the slope and intercept of the resulting line.

3. Results and Discussion

3.1. The ECCMs Morphology and Element Distribution

The SEM approach enables a visual examination of the dispersion of the ECCM. The micrographs of the surfaces of ECCMs were obtained using a JEOL JCM-7000 Benchtop microscope, with a chamber pressure of 1 bar. The microscope was operated at an accelerating voltage of 15 keV and a working distance of 13 mm.

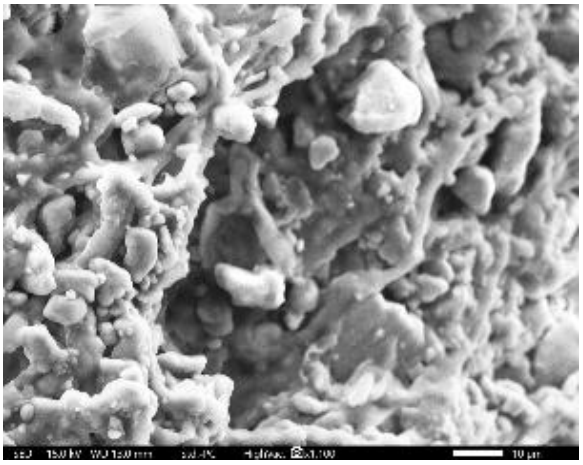

a

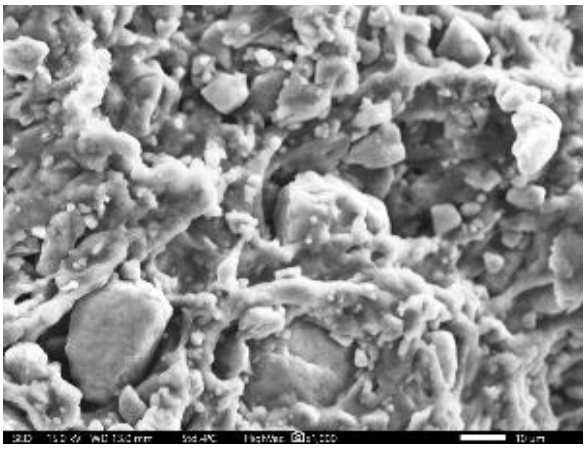

b

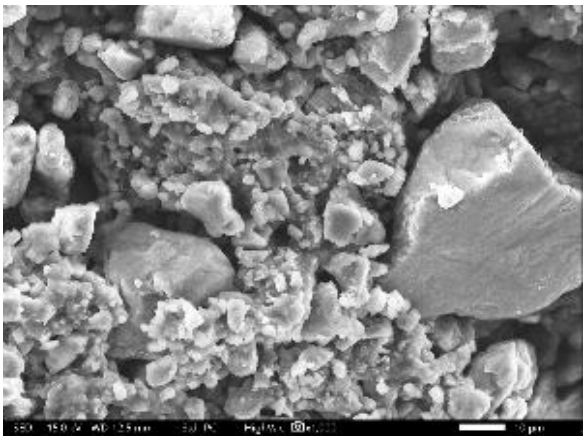

c

Fig. 2. The morphology of (a) S1, (b) S2, (c) S3 samples by SEM technique with 1000X magnification and 10 µm for scale bar

The microscope images of the S1, S2, and S3 samples revealed the presence of sizable particles that had an affinity for the AP compound. The oxidizer particles, along with the aluminium, and other components, were found to be dispersed haphazardly inside the polymeric matrix, as depicted in Fig. 2a, Fig. 2b, Fig. 2c respectively. Meanwhile, low molecular weight plasticizers molecules must be inserted between binder macromolecular chains, enabling their separation and enhancing flexibility, which is not visible in SEM pictures. The AP crystals, which are coarse crystallines, function as the oxidizer, while the PVC material surrounding them acts as both the binder and a fuel for the ECCM. The AP coarse crystallines have a random distribution and are strongly linked together by the smooth PVC matrix. In addition, the aluminium particles included in the ECCMs are easily visible and are evenly spread within the pocket region created by the AP.

Meanwhile, Fig. 3 displays the SEM image of the S4 surfaces. These surfaces were treated with a nano Fe_2O_3 energy addition. The SEM micrograph clearly reveals a uniform distribution of the burning catalyst inside the binder matrix, with nanoparticles of varying sizes. The aggregates of the S4 sample display a structure that is nearly identical to the catalyst-free materials, indicating that the inclusion of nano Fe_2O_3 did not impact the ECCM structure.

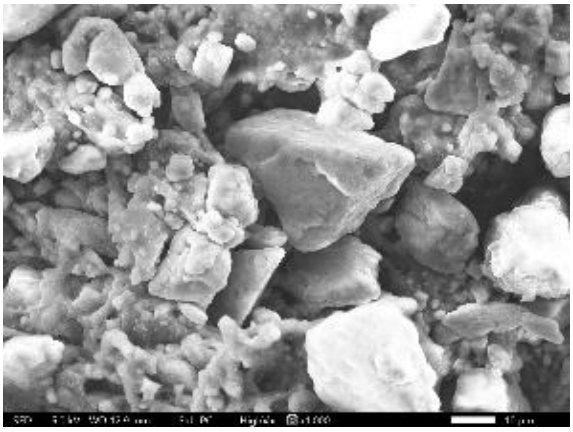

a

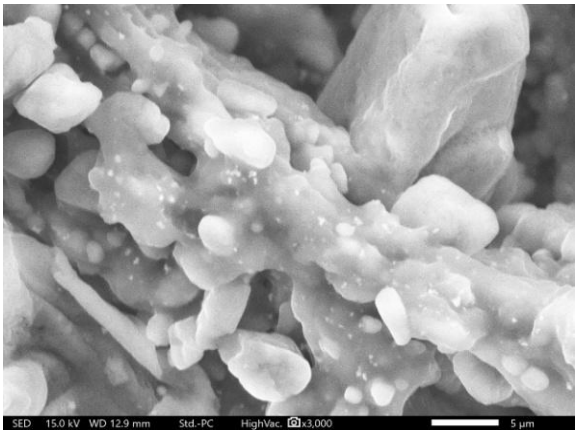

b

Fig. 3. The morphology of S4 samples by SEM technique with 1000X magnification and (a) 10 µm and (b) 5 µm for scale bar

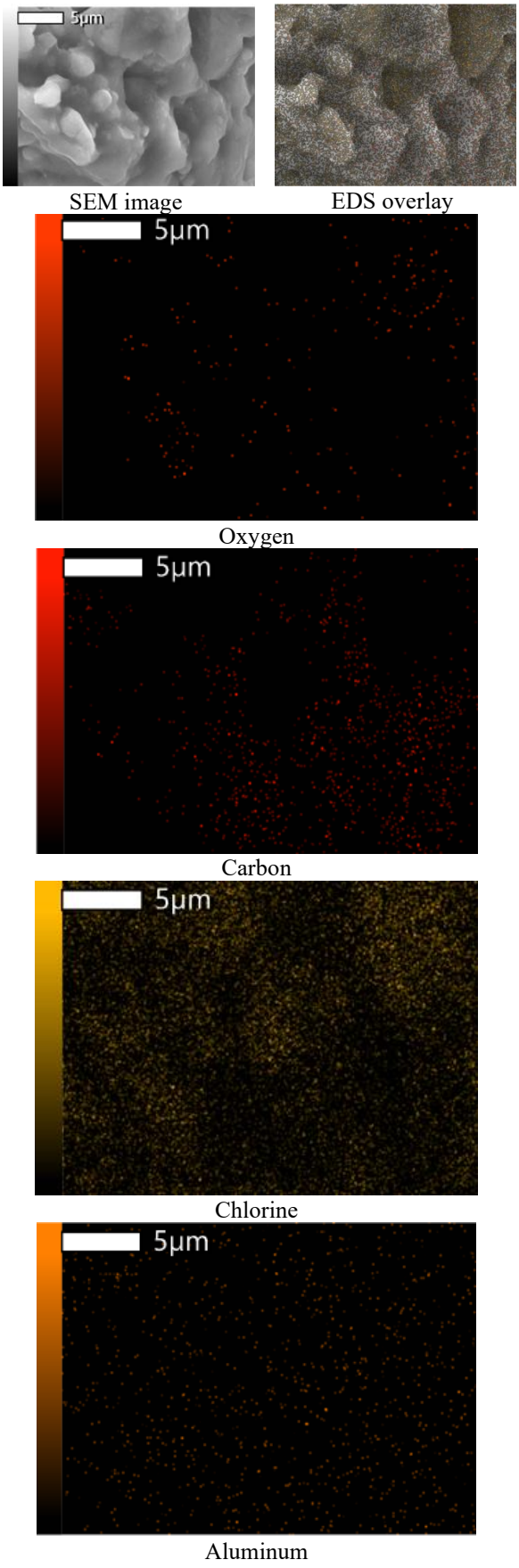

Fig. 4. EDS mapping of S2 sample

The compositional analysis of these samples was conducted using EDS, enabling the detection, identification, and quantification of elements through their unique X-rays. The metal loading in all samples, as determined by the EDS method (Table 2) analysis, closely matches the theoretical metal content calculated for ECCM manufacture. The EDS color mapping approach is used to indicate the position of each element. This method is helpful in estimating the level of ingredient dispersion on the surface of the ECCMs cross-section.

Table 2. The metals loading of the ECCM samples by EDS method

	S1	S2	S3	S4
Al (wt.%)	6.95	7.24	7.05	6.89
Fe (wt.%)	-	-	-	1.42

Refer to Fig. 4 and Fig. 5 for a visual representation of the S2 and S4 samples, respectively. The authenticity of the AP and PVC is verified through the use of EDS chlorine analysis. At the beginning of the plateau, the surface seems uneven due to the presence of clearly visible raised AP particles, while the fine AP is coated with a layer of melted PVC binder. Furthermore, it is necessary for chlorine and oxygen to be present in the same area since they are both found in AP. However, in addition to chlorine, carbon should also be present in the PVC binder, albeit in varying proportions. The aluminium particles, which have a spot size in the range of microns, were successfully collected and appeared to be adequately distributed. Simultaneously, EDS color mapping confirmed that nanoparticles of Fe_2O_3 in S4 sample exhibited ultra-fine particles with uniform size and excellent dispersion on the ECCM surface.

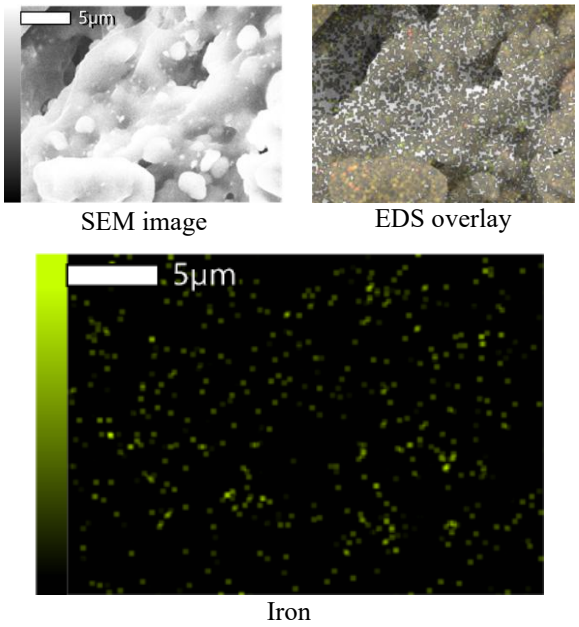

Fig. 5. EDS mapping of S4 sample

Dispersion is a crucial control parameter for both AP and, particularly, for catalytic additives. Uneven distribution of fuel and oxidizer can have a detrimental effect on combustion efficiency due to the occurrence of both fuel-rich and fuel-lean combustion in a single sample. The objective is to achieve a nearly uniform dispersion [9].

3.2. The Effect of AP Content on the ECCMs Characteristics

Modifying the AP contents, specifically the solid contents of ECCM, is optimal for altering the burn rate and combustion characteristics of ECCM. Adjusting the AP contents may negatively impact the performance of the ECCM. The TG and DSC studies of ECCMs having different oxidizer loading without Fe_2O_3 as the catalyst at a heating rate of 10 °C/min [8] has been shown in Fig. 6. The sample underwent separate reaction processes at each stage, resulting in the occurrence of multiple endothermic and exothermic peaks on the DSC curve. By analyzing the TG curve in this temperature range, it is feasible to distinguish three separate stages: Stage I, Stage II, and Stage III. These stages correspond to temperature ranges of 100-280 °C, 280-330 °C, and 330-500 °C, respectively. During the first stage, there was a 20% decrease in mass. In the second stage, there was a 17% decrease in mass. Finally, in the third stage, there was a 62% decrease in mass, resulting in only 1% left after decomposition. Nevertheless, in the instance of the S3 sample, which consisted of 80 wt.%, there was still a residual amount of up to 4%.

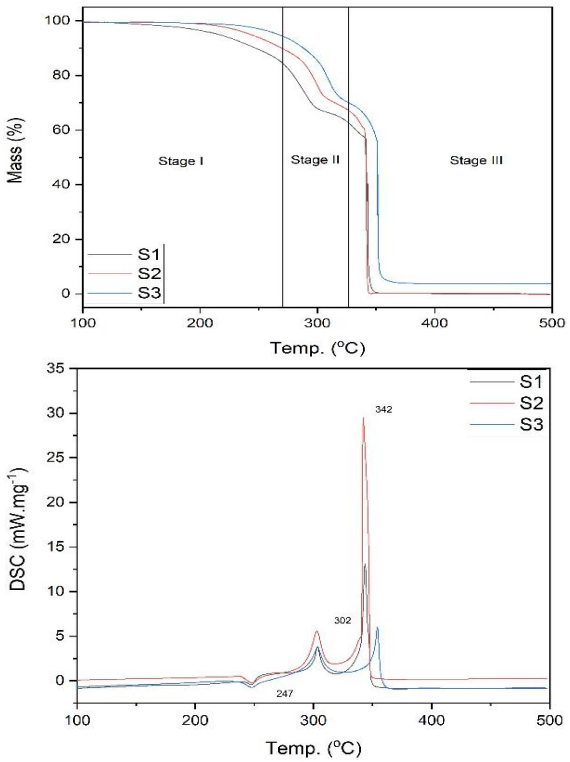

Fig. 6. Comparison of STA graph showing TG (top)/DSC (bottom) of ECCMs having different oxidizer loading

The AP, which acts as the oxidizer and main component in the ECCMs, had a significant influence on the overall thermal decomposition characteristics of the sample. Therefore, the TG/DSC curves exhibited key attributes of AP decomposition during these three phases. It is widely believed that the initial phase of AP decomposition involves the transportation of protons [10].

The perfect mechanism of AP thermal decay has been proposed by Yu Zongxue's [11]. Main AP decomposition products include NH_3 and $HClO_4$. The AP thermal decomposition is so complicated; it depends on combustion temperature.

$$NH_4ClO_4 \rightarrow NH_4^+ + ClO_4^- \quad (2)$$

$$NH_4^+ + ClO_4^- \rightarrow NH_{3(g)} + HClO_{4(g)} \quad (3)$$

$$4\,HClO_4 \rightarrow 2\,ClO_3 + 2\,ClO + 3\,O_2 + 2\,H_2O \quad (4)$$

$$2\,NH_3 + 2\,O_2 \rightarrow N_2O + 3\,H_2O \rightarrow 4\,NH_4NO_3 + H_2O \quad (5)$$

Stage I was distinguished by a peak in endothermic activity and a minor reduction in bulk. The endothermic peak at 247 °C signifies the shift of AP from an orthorhombic to a cubic shape. This transition is a crystalline phase process and does not involve any loss of mass [12]. The observed endothermic peak closely matched the findings of the earlier study [13]. The initial weight reduction seen at approximately 205 °C primarily resulted from the volatilization or decomposition of performance-enhancing substances, such as plasticizers [14].

It is widely accepted that AP undergoes a two-step decomposition process following the crystalline phase transition, specifically, low-temperature and high-temperature decomposition. In Fig. 6, the two steps are labelled as Stage II and Stage III, respectively. The exothermic peak observed at around 302 °C is attributed to the partial breakdown of AP and the generation of intermediate compounds [15]. The exothermic peak at a higher temperature (342 °C) was mainly caused by the decomposition of all residual AP and the intermediates. According to a previous report [16], the degradation of PVC consisted of two phases of mass reduction. When PVC decomposes in the presence of heat, it releases HCl in the initial stage as well as a polymer chain that contains less chlorine and light hydrocarbons in the subsequent stage. During Stage II and Stage III of the decomposition process, there was a significant mass loss of up to 79% due to the consumption of all AP, a portion of PVC, and certain additional additives. According to Wang et al., the exothermic peak at 342 °C on the DSC curve was the most intense, suggesting that the thermal degradation process of AP and PVC was accelerated during Stage III [17]. As the temperature increases, the decomposition rates of AP and PVC accelerate, resulting in the release of significant amounts of heat and the production of various types of complete oxidizing gasses. The presence of a chlorine atom in the PVC

structure facilitates the formation of chlorine-oxygen species upon reaction with AP products [16]. These compounds exhibit more reactivity than oxygen and may interact with hydrocarbons more efficiently in the subsequent step. The complete oxidizing gasses reacted with PVC, resulting in the production of heat and further accelerated the thermal degradation of AP and PVC [16].

As the AP content increased, the combustion efficiency of the ECCM first improved before declining. This phenomenon was ascribed to the combined impact of AP breakdown, which concurrently produced oxidizing gasses and intensified combustion instability in the ECCM.

3.3. The Effect of Fe_2O_3 Catalyst on the ECCMs Characteristics

The Fig. 7 displays the TG/DSC plots of the ECCM samples, comparing the ones with Fe_2O_3 as a catalyst (S4) and without a catalyst (S2). Based on the survey of different AP loadings, it was found that the S2 sample exhibited the most favorable findings in terms of thermal decomposition and exothermic qualities. Therefore, a 70 wt.% AP content was selected to study the impact of Fe_2O_3 as an energy addition. The thermal decomposition temperature of Fe_2O_3 is lower compared to uncatalyzed ECCM. In this temperature range, the TG curve exhibits three distinct stages, with only 3% remaining after decomposition. In comparison to the S2 sample, the exothermic decomposition peaks observed in the DSC plot have migrated from 342 °C to 294 °C and from 302 °C to 257 °C.

The DSC analysis of the S2 sample consisted of three primary stages, as outlined in Section 3.2. Firstly, an endothermic decomposition occurred at a temperature of 247 °C, accompanied by the absorption of 51.2 J/g of heat. Secondly, a partial exothermic decomposition took place at 302 °C, resulting in the release of 232.2 J/g of heat. Finally, the main exothermic decomposition occurred at 342 °C, with a heat release of 544.9 J/g. On the contrary, the effectiveness of ferric oxide as a catalyst for ECCM by S4 sample can be summarized as follows: the disappearance of the endothermic decomposition and the division of the partial exothermic decomposition peak into two peaks, resulting in a total heat release of 207.7 J/g. The main exothermic decomposition occurs at 294 °C, with a heat release of 649.5 J/g.

Ferric oxide offered superior catalytic activity with dramatic change in ECCM thermal behavior. According to a previous report [18], the presence of a catalyst can facilitates the production of O_2 and the absorption of gas on its surface. These investigations conclude that Fe_2O_3 is suggested to influence AP condensed phase processes, hence affecting the reactants transitioning into the gas phase. While their behavior is analogous in AP, they demonstrate distinct behavior in the binder due to Fe_2O_3 diminishing the binder's melt flow [19]. Moreover, the existence of a partially occupied third orbital in Fe^{3+} facilitates the electron transfer process, allowing the positive hole to receive electrons from AP ions and enhance thermal breakdown [20], which can be depicted by the following equations:

$$NH_4ClO_4 \rightarrow NH_4^+ + ClO_4^- \quad (6)$$

$$NH_4^+ + ClO_4^- \rightarrow ClO_4 + NH_4 \quad (7)$$

$$Fe_3^+ + ClO_4^- \rightarrow Fe_2^+ + ClO_4 \quad (8)$$

$$Fe_2^+ + NH_4^+ \rightarrow Fe_3^+ + NH_4 \quad (9)$$

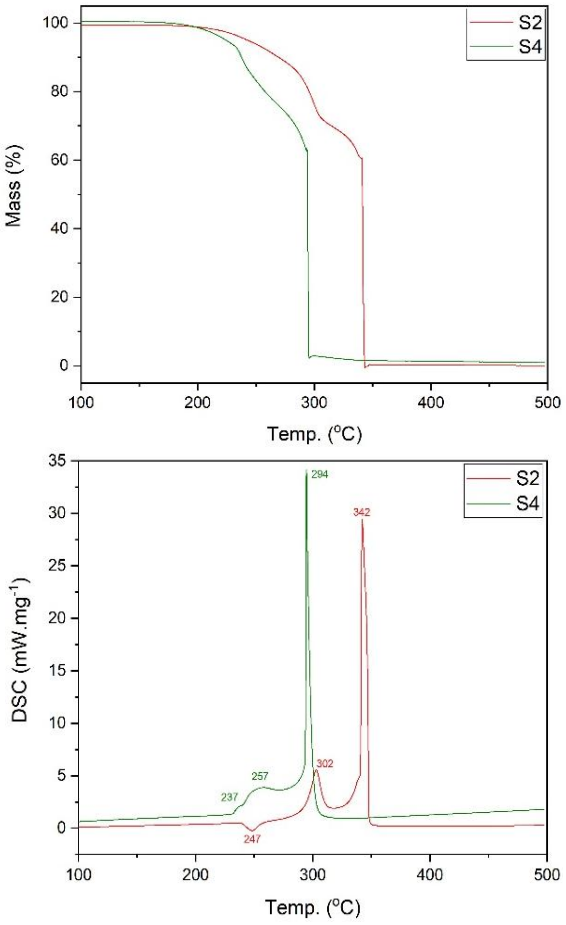

Fig. 7. Comparison of STA graph showing TG (top)/DSC (bottom) of ECCMs with and without Fe_2O_3

This activity has the potential to facilitate the accomplishment of AP thermal decomposition. Consequently, the presence of Fe_2O_3 nanoparticles led to an acceleration of the rapid advancement of AP thermal decomposition.

3.4. Burning Rate Study of AP-PVC Based ECCMs

The combustion rate results of ECCMs based on AP as an oxidizer and PVC as a fuel binder, with and without Fe_2O_3, are illustrated in Table 3 and Fig. 8. The burning rates were depicted as a function of pressures,

and the curves illustrate the impact of the Fe_2O_3 nanoparticles on the evolution of the burning rate with pressure.

Table 3. Burning rate of ECCM S2 and S4 at different pressures

Sample	S2	S4
Pressure (MPa)	Burning rate (mm/s)	
0.109	2.067	2.115
2.595	5.431	7.357
5.073	6.104	8.975
6.395	6.328	9.553
7.993	6.493	10.035
a	3.983	5.015
n	0.273	0.309

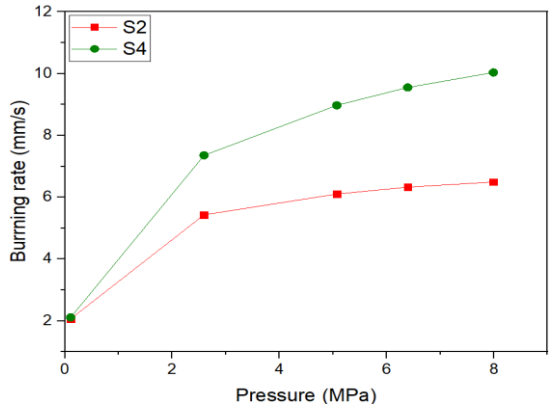

Fig. 8. Evolution of the burning rate with pressure for ECCMs corresponding with and without Fe_2O_3

Pressure exponent n is more critical because it determines how rapidly the burning rate changes with pressure while coefficient a becomes crucial as it establishes the base burning rate. Indeed, the combustion rate, the coefficient a and the pressure exponent n are significantly influenced by the impact of Fe_2O_3. The results obtained are a strong confirmation of the law that the burning rate is directly proportional to the pressure in the combustion chamber. The combustion flow stability condition, which is determined by the pressure exponent n ($n < 1$), has been confirmed (n = 0.273 for the ECCM that was constructed without Fe_2O_3 (S2) and n = 0.309 for the ECCM that was elaborated from Fe_2O_3 (S4), as illustrated in experimental data). Table 3 and Fig. 8 demonstrate that by presence of Fe_2O_3, S4 exhibited higher combustion rates than S2, in addition to having a higher n, which is consistent with the literature [21]. The Saint-Robert's Law equation for S2 and S4 ECCM samples should be displayed as bellow:

$$For\ S2:\ r = 3.983P^{0.273} \quad (10)$$

$$For\ S4:\ r = 5.015P^{0.309} \quad (11)$$

4. Conclusion

In this work, the thermal decomposition characteristics of ECCMs were studied. The influence of oxidizer content and energy additive were analyzed. The key findings are summarized as follows:

1. The SEM is an effective instrument for analyzing the composition of ECCMs. These high-resolution, high-depth-of-focus photos illustrate the AP content and catalytic additives influencing combustion. The matrix may be observed melting over the particles and the artifacts accumulating in the AP particle. EDS is crucial since it facilitates the identification of these artifacts and provides an accurate ratio of AP components on the surface.
2. The thermal decomposition process of the ECCM was found to consist of three distinct stages, as determined by TG/DSC analysis. The rate at which mass was lost during the process, ranging from 100 °C to 500 °C, reached a remarkable 99% for samples containing 70 wt.% of AP. This significant mass loss was primarily caused by the decomposition of AP. The peak at 247 °C, which absorbs heat, and the peaks at 302 °C and 342 °C, which release heat, are connected to the changes in the crystal structure, decomposition at low temperatures, and decomposition at high temperatures of AP, respectively. AP content climbed, ECCM combustion efficiency first improved (70 wt.%) then declined (80 wt.%). AP breakdown caused oxidizing fumes and increased combustion instability in the ECCM.
3. Experiments are conducted to investigate the behavior of iron oxide in the presence of AP and binder within an ECCM. The ferric oxide particles demonstrated enhanced catalytic activity by reducing the exothermic decomposition of ECCM to a lower temperature. In addition, Fe_2O_3 exhibited distinct thermal characteristics for AP particles, resulting in a significant increase of around 10% in total heat release.
4. The burning rate is significantly increased with the same AP loading when the burning catalyst Fe_2O_3 is added at a concentration of 1.5 wt.%, particularly in the high-pressure region. The burning rate of S2 and S4 samples are displayed by Saint-Robert's Law equation.

Despite a direct correlation between the AP content and the PVC content in the ECCMs, it is imperative to conduct several control experiments that vary only the PVC content while maintaining all other components constant. This will elucidate the precise impact of PVC content on combustion characteristics and clarify its role in the combustion process. The mechanical characteristics of the composite, which dictate its possible uses, are significantly affected by the PVC content and the presence of plasticizers, aspects that

have not been extensively examined. All these factors will investigate in our further research.

References

[1] G. P. Sutton, O. Biblarz, Rocket Propulsion Elements, Hoboken, NJ, USA: John Wiley & Sons, 2016, pp. 75–95.

[2] A. Manash, P. Kumar, Comparison of burn rate and thermal decomposition of AP as oxidizer and PVC and HTPB as fuel binder based composite solid propellants, Defence Technology, vol 15, no. 2, pp. 227–232, Apr. 2019. https://doi.org/10.1016/j.dt.2018.08.010

[3] K. Ganesh, S. Sundarrajan, K. Kishore, K. N. Ninan, B. George, M. Surianarayanan, Primary pyrolysis products of hydroxy-terminated polybutadiene, Macromolecules, vol. 33, pp. 326–330, Dec. 1999. https://doi.org/10.1021/ma990423p

[4] N. Kubota, Propellants and Explosives: Thermochemical Aspects of Combustion, 3rd Edition, Weinheim, Germany: John Wiley & Sons, pp. 69–112, 2007.

[5] V. V. Boldyrev, Thermal decomposition of ammonium perchlorate, Thermochimica Acta, vol. 443, no. 1, pp. 1–36, Apr. 2006. https://doi.org/10.1016/j.tca.2005.11.038

[6] J. Yuan, J. Liu, Y. Zhou, Y. Zhang, K. Cen, Thermal decomposition and combustion characteristics of Al/AP/HTPB propellant, Journal of Thermal Analysis and Calorimetry, vol. 143, pp. 3935–3944, Feb. 2020. https://doi.org/10.1007/s10973-020-09297-4

[7] P. R. Prajakta, V. N. Krishnamurthy, S. Joshi Satyawati, Differential scanning calorimetric study of HTPB based composite propellants in presence of nano ferric oxide, Propellants, Explosives, Pyrotechnics, vol. 31, pp. 234–241, Dec. 2006. https://doi.org/10.1002/prep.200600059

[8] C. Dennis, B. Bojko, On the combustion of heterogeneous AP/HTPB composite propellants: a review, Fuel, vol. 254, pp. 115646–115651, Oct. 2019. https://doi.org/10.1016/j.fuel.2019.115646

[9] G. R. Morrow, A. R. Demko, and E. L. Petersen, Modern scanning electron Mmcroscopy in the study of solid propellant combustion: surface structure and elemental identification via EDS, AIAA 2016–4594, Session: Propellant Development - Solid Fuel, Jul. 2016. https://doi.org/10.2514/6.2016-4594

[10] N. Yadav, P. K. Srivastava, M. Varma, Recent advances in catalytic combustion of AP-based composite solid propellants, Defence Technology, vol. 17, no. 3, pp. 1013–1031, Jun. 2021. https://doi.org/10.1016/j.dt.2020.06.007

[11] J. A. Vara, P. N. Dave, S. Chaturvedi, The catalytic activity of transition metal oxide nanoparticles on thermal decomposition of ammonium perchlorate, Defence Technology, vol. 15, no. 4, pp. 629–635, Aug. 2019. https://doi.org/10.1016/j.dt.2019.04.002

[12] L. Mallick, S. Kumar, A. Chowdhury, Thermal decomposition of ammonium perchlorate–A TGA-FTIR-MS study: Part II, Thermochimica Acta, vol. 653, Jul. 2017, pp. 83–96. https://doi.org/10.1016/j.tca.2017.04.004

[13] M. B. Padwal, M. Varma, Thermal decomposition and combustion characteristics of HTPB-coarse AP composite solid propellants catalyzed with Fe_2O_3, Combustion Science and Technology, vol. 190, pp. 1614–1629, Mar. 2018. https://doi.org/10.1080/00102202.2018.1460599

[14] D. Trache, F. Maggi, I. Palmucci, L. T. DeLuca, Thermal behavior and decomposition kinetics of composite solid propellants in the presence of amide burning rate suppressants, Journal of Thermal Analysis and Calorimetry, vol. 132, pp. 1601–1615, Mar. 2018. https://doi.org/10.1007/s10973-018-7160-8

[15] L. Liu, J. Li, L. Zhang, S. Tian, Effects of magnesium-based hydrogen storage materials on the thermal decomposition, burning rate, and explosive heat of ammonium perchlorate-based composite solid propellant, Journal of Hazardous Materials, vol. 342, pp. 477–481, Jan. 2018. https://doi.org/10.1016/j.jhazmat.2017.08.055

[16] A. AI-Harthi, A. Williams, Effect of fuel binder and oxidiser particle diameter on the combustion of ammonium perchlorate based propellants, Fuel, vol. 77, no. 13, pp. 1451-1468, Oct. 1998. https://doi.org/10.1016/S0016-2361(98)00059-3

[17] Y. Wang, L. Liu, L. Xiao, Z. Wang, Thermal decomposition of HTPB/AP and HTPB/HMX mixtures with low content of oxidizer, Journal of Thermal Analysis and Calorimetry, vol. 119, pp. 1673–1678, Dec. 2014. https://doi.org/10.1007/s10973-014-4324-z

[18] S. Elbasuney, M. Yehia, Ferric oxide colloid: a novel nano-catalyst for solid propellants, Journal of Inorganic and Organometallic Polymers and Materials, vol. 30, pp. 706–713, Nov. 2019. https://doi.org/10.1007/s10904-019-01339-1

[19] K. Ishitha, P.A. Ramakrishna, Studies on the role of iron oxide and copper chromite in solid propellant combustion, Combustion and Flame, vol. 161, no. 10, pp. 2717–2728, Oct. 2014. https://doi.org/10.1016/j.combustflame.2014.03.015

[20] Y. Zhang, X. Liu, J. Nie, L. Yu, Y. Zhong, C. Huang, Improve the catalytic activity of α-Fe2O3 particles in decomposition of ammonium perchlorate by coating amorphous carbon on their surface, Journal of Solid State Chemistry, vol. 184, no. 2, pp. 387–390, 2011. https://doi.org/10.1016/j.jssc.2010.12.004

[21] A. Amir, A. W. K. Wan, Effect of oxidizer-fuel mixture ratio to the pressure exponent of ammonium perchlorate based composite propellant, Applied Mechanics and Materials, vol. 110, no. 116, 2012, pp. 1380–1386. https://doi.org/10.4028/www.scientific.net/AMM.110-116.1380